Studia Geophysica et Geodaetica (2026) 70:8
https://doi.org/10.1007/s11200-026-00018-5

Magnetic fabrics and paleomagnetism of continental mudrocks: Implications for unravelling the tectonic evolution of the South Pyrenean Zone (NE Spain)

Pablo Sierra-Campos[1,2] · Pablo Calvín[3] · Esther Izquierdo-Llavall[1,2] · Manuel Montes[4] · Aránzazu Luzón[2,5] · Eva Bellido[4] · Elisabet Beamud[6] · Emilio L. Pueyo[1,2] · Juan Cruz Larrasoaña[1,2,7]

Received: 12 August 2025 / Accepted: 24 October 2025

Abstract

The anisotropy of the magnetic susceptibility (AMS) in mudrocks has been widely used to study orogenic belts due to their sensitivity to strain, while paleomagnetism remains the most effective method to quantify vertical axis rotations (VARs) resulting from the accommodation of along-strike variations in shortening. However, AMS can be also eventually used as a passive marker to detect VARs and the integration of both techniques offers a powerful approach to understand the tectonic evolution of fold-and-thrusts-belts. In this work, a combined AMS and paleomagnetic study along a stratigraphic section of continental rocks from the Campodarbe Formation in the Jaca-Pamplona Basin, southern Pyrenees, was carried out. This stratigraphic section (Martes section) records the tectonic evolution of this part of the basin from Priabonian to Rupelian times. The magnetic fabrics show the imprint of early stages of deformation, characterized by dominantly oblate ellipsoids and WNW-ESE horizontal magnetic lineations (axes of maximum magnetic susceptibility k_{max}), parallel to bedding and the main regional structures. In the lower part of the section, k_{max} axes trend around 290º, gradually rotating to 270º towards the top. The AMS is interpreted as locked under the imprint of the layer parallel shortening (LPS) associated to the activity of the basement thrusts in the northern Jaca-Pamplona Basin. On the other hand, paleomagnetic data indicate clockwise VARs of 6º to 12º in the lower part of the section, and a counterclockwise rotation of 7º to 14º in the upper part. These differential rotations could result from lateral changes in the Biniés basement thrust or the Jaca thrust system that were active during Oligocene times. Both techniques record a net rotation of ca. 25º between the lower and upper part of the section, which support the interpretation that early-locked AMS behaves as a passive marker and validates its use for detecting and quantifying VARs.

Keywords AMS · Paleomagnetism · Vertical axis rotations · LPS · Jaca-Pamplona Basin

Extended author information available on the last page of the article

Published online: 03 April 2026

1 Introduction

The anisotropy of the magnetic susceptibility (AMS) in mudrocks has made timely contributions to the study of orogenic regions and foreland basins due to its sensitivity to detect the preferred orientation of phyllosilicates in relation to strain in compressive settings (Tarling and Hrouda, 1993; Borradaile and Jackson, 2004, 2010). This is particularly evident in the case of weakly deformed mudrocks that display no mesoscopic-scale evidence of strain. The study of their magnetic fabrics has furnished our understanding of the external portions of orogens and neighbouring foreland basins that, by virtue of their low deformation degree, would have remained otherwise understudied and poorly integrated in their wider tectonic contexts (Graham, 1954; Nye, 1957; Hrouda, 1982; Tarling and Hrouda, 1993; Borradaile and Henry, 1997; Borradaile, 2001; Borradaile and Jackson, 2004, 2010; Parés, 2004, 2015). The ability of magnetic fabrics to record deformation at low stress conditions emerges from the relationship that exists between the magnetic and the crystallographic anisotropy axes of the phyllosilicates (Martín-Hernández and Hirt, 2003), and their subsequent evolution upon deformation (Parés et al., 1999; Parés, 2004, 2015; Soto et al., 2009; Larrasoaña et al., 2011). Magnetic susceptibility is an intrinsic property of the matter that relates the orientation, sign and intensity of the magnetization of a substance acquired under an external magnetic field and the strength of that field, for a given temperature (Nye, 1957; Tarling and Hrouda, 1993). The AMS, a second rank tensor, is represented by an ellipsoid that changes in orientation and shape according to the registered stress, being a sensitive marker for studying the evolution of fold-and-thrust systems and foreland basins (Hrouda and Janák, 1976; Hrouda, 1979; Hrouda and Kahan, 1991; Borradaile and Henry, 1997; Parés, 2004, 2015; Pueyo-Anchuela, et al., 2011). According to most Authors, sediments in foreland domains record an initial sedimentary fabric enhanced by compaction. This fabric displays an oblate ellipsoid that is parallel to bedding, with no preferential arrangement of the maximum susceptibility k_{max} axes within the bedding plane in response to the random settling of phyllosilicates under the typical low-energy conditions that characterize the deposition of marls (the so-called Type I fabric of Parés, 2015). Increased stress conditions force phyllosilicates to undergo an initial, subtle rotation or minor deformation (e.g., crenulation or kinking) around a horizontal axis perpendicular to the direction of layer-parallel shortening (LPS) (Ho et al., 1995). In this context, the magnetic foliation remains parallel to bedding but a clustered magnetic lineation begins to develop perpendicularly to the LPS direction (Type IIa fabric of Parés, 2015). As deformation increases, the orientation of k_{max} enhances its clustering perpendicular to the shortening direction, marking the intersection lineation between bedding and an emerging slaty cleavage. Meanwhile, axes of the intermediate (k_{int}) and minimum (k_{min}) susceptibility form a girdle due to the superposition of cleavage planes on bedding, both contributing to the magnetic fabric. This configuration results in a prolate to triaxial ellipsoid, characteristic of a Type IIb fabric (Parés, 2015). Eventually, magnetic foliation becomes parallel to well-developed cleavage once sufficient deformation has been attained, leading to the development of an oblate ellipsoid corresponding to a Type III fabric (Parés, 2015).

The sensitivity of magnetic fabrics to detect the earlier deformation stages in mudrocks is such that they have been used, in addition to detect the earliest signs of deformation themselves, to inform on other important aspects of the tectonic evolution of orogens and foreland basins. Thus, magnetic fabrics have been used to detect blind thrusts in areas where the stratigraphic homogeneity of the mudrocks has prevented the identification and delineation of such relevant structures at a cartographic scale (Hirt et al., 2004; Boiron et al., 2020; Gracia-Puzo et al., 2021; Menzer et al., 2024; Sierra-Campos et al., 2025a). In these cases, the magnetic fabrics have been shown to reflect the evolution from Type I to Type IIa and Type IIb ellipsoids as the mudrocks get closer to thrust zones that had been previously overlooked (Hirt et al., 2004; Boiron et al., 2020; Gracia-Puzo et al., 2021; Menzer et al., 2024; Sierra-Campos et al., 2025a), with the implications it has for the accurate reconstruction of the geometry and kinematics of thrust systems.

Besides paleomagnetism, considered the most widely used technique to unravel and quantify vertical axis rotations (VARs) undergone in fold-and-thrust belts (e.g., Norris and Black, 1961; McCaig and McClelland, 1992; Allerton, 1998; Pueyo et al., 2016; and references therein), magnetic fabrics have also been shown to provide accurate estimates of VARs due to the passive behaviour that magnetic ellipsoids attain after they are locked in and subsequent faulting takes up the deformation (Sagnotti et al., 1998; Cifelli et al., 2004; Weaver et al., 2004; Pueyo-Anchuela et al., 2012).

In this work, we present the results of a combined AMS and paleomagnetic study carried out on weakly deformed mudrocks of the continental Campodarbe Formation that crop out in the central sector of the Jaca-Pamplona Basin (southern Pyrenees, NE Spain). The importance of this area lies in the fact that it is located within the region where clockwise VARs documented in the eastern part of the basin (Pueyo-Anchuela et al., 2012; Mochales et al., 2012; Rodríguez-Pintó et al., 2016; Pueyo et al., 2022) dampen towards the west (Larrasoaña et al., 2003; Oliva-Urcia et al., 2012; Pueyo-Anchuela et al., 2012) in response to the changing geometry and kinematics of the South Pyrenean Frontal Thrust (Muñoz et al., 2025; Toro, 2025). Since the studied mudrocks have been collected along a 2667 m-thick section that ranges from the Late Eocene to the Early Oligocene (Hogan and Burbank, 1996; Oliva-Urcia et al., 2019; Anastasio et al., 2020), our results provide important constraints not only on the spatial distribution of VARs, but also on their timing within the context of the kinematic evolution of this part of the Central-Western Pyrenees.

2 Geological Setting

The Pyrenees are an asymmetric and doubly verging orogen that resulted from the collision between the Iberian and the European plates from the Late Cretaceous to the Early Miocene (Choukroune, 1992; Muñoz, 1992, 2002; Pedrera et al., 2023 and references therein). The Pyrenees are divided into three main domains, from north to south, the North Pyrenean, the Axial and the South Pyrenean zones, being the later limited to the south by the South Pyrenean Frontal Thrust over the Ebro foreland basin (Fig. 1). A number of studies based on legacy

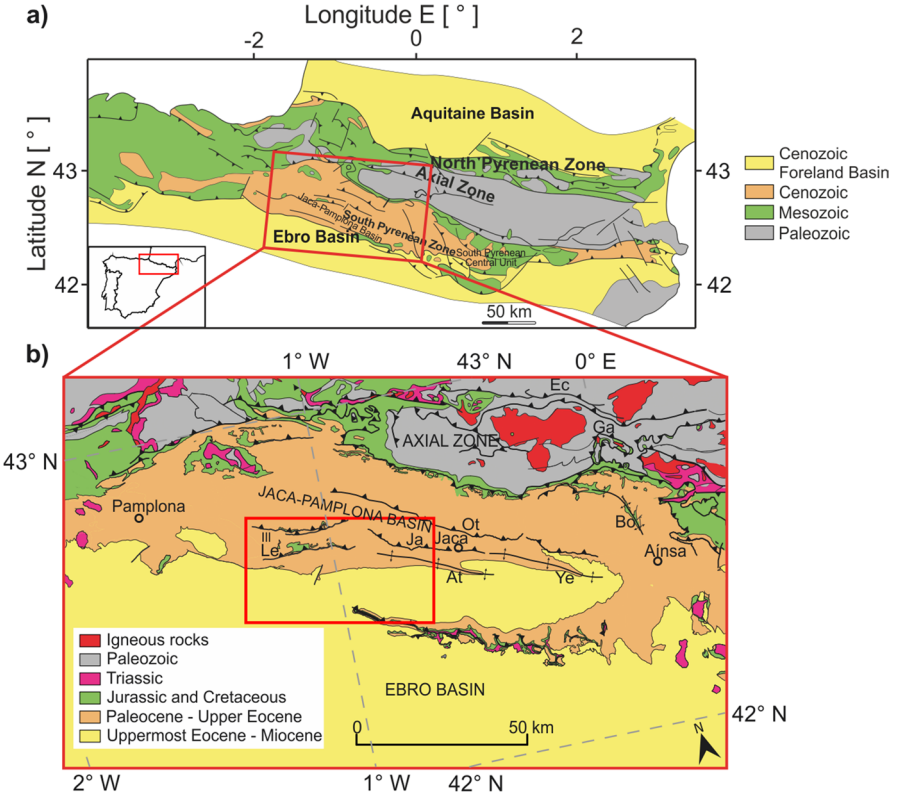

Fig. 1 **a)** Geological map of the Pyrenees with the location of the study area (modified from Teixell, 1996). **b)** Geological map of the southwestern Pyrenees with the main structures and the study area. The red rectangle is shown in detail in Fig. 2. Ec: Eaux-Chaudes thrust; Ga: Gavarnie thrust; Ot: Oturia thrust; Ja: Jaca thrust; Ill: Illón thrust; Le: Leyre thrust; Ye: Yebra de Basa anticline; At: Atarés anticline; Bo: Boltaña anticline

exploration seismic sections from the Jaca-Pamplona Basin, in the western part of the South Pyrenean Zone (SPZ), have identified a complex setting with relevant along-strike variations affecting both basement and cover structures (Cámara and Klimowitz, 1985; Labaume et al., 2016; Labaume and Teixell, 2018; Toro et al., 2021; Muñoz et al., 2025). Regarding basement geometries, early studies (Labaume et al., 1985; Teixell, 1996) provided a simplified geometry and interpreted three main, south-directed basement thrusts across the area, from north to south, the Lakora-Eaux-Chaudes, Gavarnie and Guarga thrusts (Teixell, 1998; Millán et al., 2000; Teixell et al., 2016). However, a number of additional basement structures have been interpreted recently from the review of seismic sections (Labaume and Teixell, 2018; Muñoz et al., 2025; Toro, 2025) that emphasize the existence of oblique basement thrust and a regionally non-cylindrical basement structure beneath the Jaca-Pamplona Basin. For the central Jaca-Pamplona Basin, these studies identify and trace the Biniés thrust, characterized by a

kilometric-scale, NE-SW-trending hangingwall ramp (see location in Fig. 2). In the hangingwall of Biniés, the Gavarnie thrust is imaged in seismic profiles as a complex thrust system (i.e., the Gavarnie basement thrust system) that deforms the basement beneath the southern Axial Zone and the northern Jaca-Pamplona Basin. In the footwall of Biniés, the Guarga thrust (Labaume and Teixell, 2018) ends laterally and is westwards relayed by multiple basement thrusts displaying moderate displacements (the Jaca thrust system in Muñoz et al., 2025). These basement structures connect to cover structures along multiple frictional décollements and a main viscous-type décollement represented by the Late and Middle Triassic evaporites of the Keuper and Muschelkalk units (Labaume et al., 1985; Teixell, 1996; Izquierdo-Llavall et al., 2013; Muñoz et al., 2025). The area is bounded by three main outcropping and Triassic-detached structures: the Santo Domingo anticline to the south and the Leyre and Illón thrust systems to the north (Millán, 1996). The Illón thrust connects towards the east with the folds

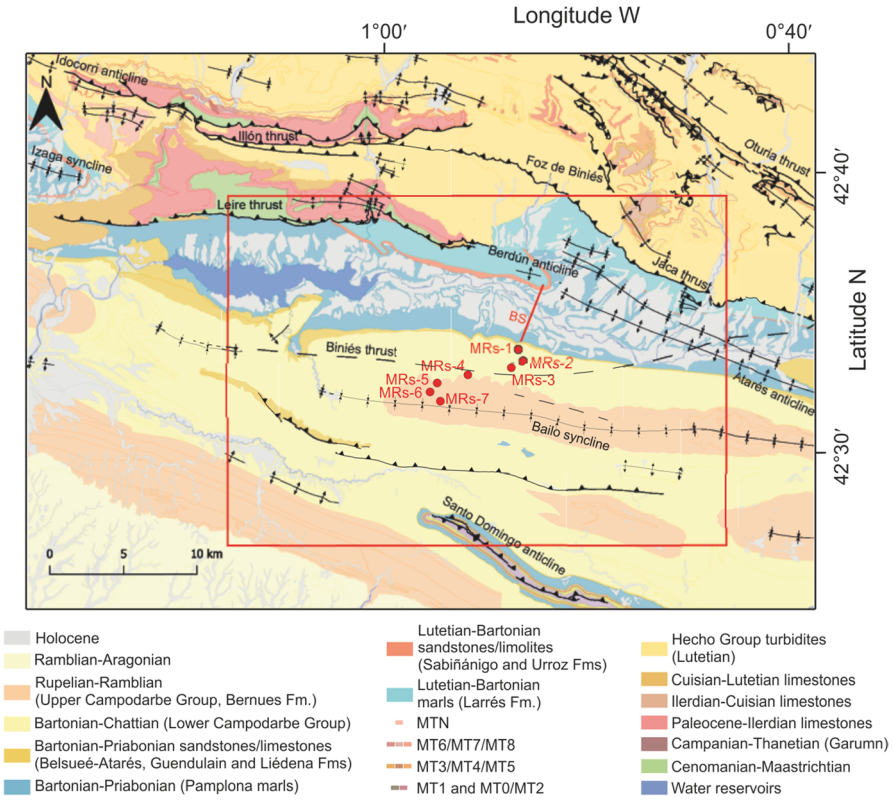

Fig. 2 Geological map of the studied area (modified from Robador Moreno et al., 2024a,b; Government of Navarre, 2024) with the main structures and the discretized sites (labelled red dots). Results obtained for the sites in the red rectangle are shown in Fig. 8. BS: Berdún section (Sierra-Campos et al., 2025a); MT: megabreccias interbedded within the Hecho Group turbidites; dashed curve: cutoff of the Biniés thrust

of the Foz of Biniés area whereas the Leyre structure can be followed to the east along the Berdún and Atarés anticlines (Fig. 2).

The along-strike differences in the magnitude of the displacement associated to the different basement and cover units explains the occurrence of a distinct pattern of vertical axes rotation (VAR) identified within the Jaca-Pamplona Basin from a recent review of paleomagnetic data (Pedrera et al., 2023 and references therein). The maximum VAR magnitudes are found at the boundary between the Jaca-Pamplona Basin and the South Pyrenean Central Unit (SPCU) to the east (Fig. 1a), where the systematic clockwise rotations of 35°–50° reported in the Aínsa oblique zone attest to a more important shortening undergone along the SPCU (Mochales et al., 2012, 2016; Muñoz et al., 2013; Rodríguez-Pintó et al., 2016). Westwards, a fairly constant CW rotation of 20°–25° is reported within the eastern and central sectors of the Jaca-Pamplona Basin and in the External Sierras front in response to a progressive, linear decrease in the amount of shortening experienced by the basin (Pueyo-Anchuela et al., 2012; Pueyo et al., 2021, 2025). The westernmost part of the basin (west of Leyre-Illón ranges; Fig. 2) displays no significant VAR (Larrasoaña et al., 2003; Oliva-Urcia et al., 2012; Sierra-Campos et al., 2025b).

The sedimentary evolution of the Jaca-Pamplona Basin has been intimately linked to its southward displacement atop of the underlying basement and cover structures developed during the building of the Pyrenean orogen. Its sedimentary infill begins in the Lutetian with the deep marine turbidites of the Hecho Group, which were fed from the emerging areas in the east (Dreyer et al., 1999; Garcés et al., 2020). As deformation migrated to the south with the activity of the Gavarnie thrust system and its shortening transference to the Oturia and Jaca cover thrusts during Bartonian and Priabonian times, the westward progradation of the sedimentary system continued with the prodeltaic marls of the Larrés, Sabiñánigo-Urroz and Pamplona formations and the deltaic facies of Belsué-Atarés and Guendulain formations (Puigdefábregas, 1975; Montes, 2009; Labaume et al., 2016; Oliva-Urcia et al., 2019). During the Priabonian (~36 Ma), sedimentation of continental rocks commenced due to the disconnection of the basin from the Atlantic Ocean, probably caused by a sea level fall and a tectonic uplift produced by the Gavarnie thrust system (Costa et al., 2010; Sierra-Campos et al., 2025a). Finally, during the deposition of the upper part of the Campodarbe Formation and the deposition of the Uncastillo Formation in the Ebro Basin in the south (Rupelian-Aquitanian times) (Millán et al., 1995, 2000), the basin was transported southward as a piggyback basin atop the Guarga basement thrust to the east and the Biniés thrust and the Jaca thrusts system across the study area (Muñoz et al., 2025).

Our study area is located in the central part of the Jaca-Pamplona Basin, to the SE of the Illón and Leyre thrusts. The area approximately coincides with the transition between the eastern and western sectors of the basin displaying significant clockwise (20°–25°) and non-significant VARs, respectively. We collected our samples along the so-called Martes section, where a thick sequence of Priabonian-Rupelian continental sediments (~3000 m) from the Campodarbe Formation crop out. This sedimentary sequence has been magnetostratigraphically dated to the south, in the Salinas and Luesia-Fuencalderas sections (Hogan and Burbank, 1996; Oliva-Urcia et al., 2019respectively). Sampling sites are located in the northern limb of the Bailo

syncline (northern sector of the Guarga synclinorium; Figs. 1 and 2), in the hanging-wall of the Biniés basement thrust and the foreland of the Gavarnie basement thrust system.

3 Methods

The Martes section was sampled in the hills near the localities of Martes and Bagüés, in the NW part of the Huesca and Zaragoza provinces (base: 42°33′55.33″N, 0°53′33.74″W; top: 42°31′35.32″N, 0°56′45.78″W). This section is a continuation of the Berdún section located further north, where the magnetic fabrics of a 2000 m thick marine succession in the area have been recently reported (Sierra-Campos et al., 2025a). The Martes section is composed of continental rocks, mostly mudstones and siltstones, with frequent intercalations of fine- and coarse-grained sandstones, that belong to the Campodarbe Formation (Fig. 2). Two to three oriented paleomagnetic samples were collected at 169 stratigraphic positions evenly distributed along the 2667 m thick section, focusing on the mudstones and siltstones. The samples were drilled using a portable electrical power drill cooled by water and the sampled cores were oriented in situ with a magnetic compass adapted in a core-orienting fixture. The cores were cut into standard paleomagnetic specimens in the Magnetic Fabrics Laboratory at the University of Zaragoza (Geotransfer Research Group). In total, the AMS of 249 specimens was measured using a KLY-5A Kappabridge (AGICO, Czech Republic) with an applied field of 400 A m^{-1} and a frequency of 1220 Hz. Statistics of Jelínek (1978) was applied by means of the Anisoft 6.1.02 software (Chadima et al., 2024) allowing for estimation of the average orientation of the AMS axes. The AMS ellipsoid is defined by the three main axes of the susceptibility matrix ($k_{\max} \geq k_{int} \geq k_{min}$), where k_{max} defines the magnetic lineation and k_{min} represents the pole of the magnetic foliation (Hrouda, 1982). Scalar parameters derived from the ellipsoid axis were also estimated; the mean susceptibility (k_m), the corrected degree of anisotropy (P') and the shape parameter (T), defined as (Jelínek, 1981):

$$k_m = \frac{k_{max} + k_{int} + k_{min}}{3}, P' = P^a = \left(\frac{k_{max}}{k_{min}}\right)^a,$$

$$a = \sqrt{1 + \frac{T^2}{3}}, T = \frac{2\ln k_{int} - \ln k_{max} - \ln k_{min}}{\ln k_{max} - \ln k_{min}}$$

To characterize the magnetic properties of the sampled material, the temperature dependence of the magnetic susceptibility was evaluated using the KLY-3 and CS-3 devices (AGICO, Czech Republic) at the Magnetic Fabrics Laboratory of the University of Zaragoza and interpreted with the Cureval 8 software (Chadima and Hrouda, 2012). The percentage of paramagnetic behavior was calculated from room temperature to 250 °C using the method developed by Hrouda et al. (1997), which is incorporated into the Cureval 8 software.

Stepwise demagnetization and measurement of the natural remanent magnetization (NRM) was conducted in the Paleomagnetic Laboratory of the Geo3BCN (CCiTUB-GEO3BCN-CSIC) in Barcelona. One specimen per site was thermally demagnetized using a furnace with separated heating and cooling chambers (ASC TD48EU, ASC Scientific). A superconducting rock magnetometer (2G Enterprises) with a noise level of $< 7 \times 10^{-6}$ A m^{-1} was used to measure the NRM from room temperature to 680 °C, with at least thirteen steps of 50 °C to 10 °C heating increments. Low-field magnetic susceptibility was also monitored to detect the neoformation of magnetic minerals upon heating using a KLY-2 Kappabridge (AGICO, Czech Republic). The VPD software (Ramón et al., 2017) was used to calculate the paleomagnetic direction of the characteristic remanent magnetization (ChRM) by principal component analyses (PCA, Kirschvink, 1980), after visual inspection and manual selection of steps from the orthogonal demagnetization plots (Zijderveld, 1967).

Since the data come from a succession studied also for magnetostratigraphic purposes, a discretization routine was implemented to determine the evolution of VARs along the section as previously done in other Pyrenean sections (Mochales et al., 2012). To do so, the mean paleomagnetic directions of successive 400 m thick intervals (MRs-1 to MRs-7) were calculated averaging all the available paleomagnetic directions after applying the following quality criteria i) only ChRMs directions with maximum angular deviation (MAD) angles < 17° were used; ii) only subsequent virtual geomagnetic poles (VGP) with latitude ≥ 30° and ≤ –30° were considered, iii) finally, south directions with positive inclinations (and the contrary) were ruled out from further calculations. Reverse ChRM directions were converted into their antipodal directions and all the data were processed in the lower stereographic hemisphere. The Stereonet software (Allmendinger et al., 2013) was used to apply standard Fisher (1953) statistics. Geographic coordinates, bedding attitude and NRM were also averaged out. To calculate VARs, paleomagnetic declinations were compared with the relevant (Eocene–Oligocene) Iberian reference direction compiled by Pedrera et al. (2023) (number of samles $n = 119$; declination $D = 2.3°$; inclination $I = 42.8°$; 95% confidence interval $\alpha_{95} = 2.2°$; Fisher's (1953) concentration parameter $\kappa = 38.1$; and the resultant length $R = 0.9740$), and associated uncertainties in VARs derived from the α_{95} of the paleomagnetic directions were assessed by $\Delta D = \alpha_{95}/\cos I$ (Demarest, 1983).

The magnetic fabric results have been also discretized following a similar procedure, that is, averaging the relevant scalar (k_m, P' and T) and directional (k_{max} direction) data along the same 400 m thick intervals. Average k_m, P' and T data have been calculated along with their respective standard deviations σ, whereas average k_{max} directions and associated errors have been calculated using statistics of Jelínek (1978) as included in the Chadima et al. (2024) software.

4 Results

4.1 Magnetic Fabrics

The mean susceptibility (k_m) of the Martes dataset ranges between 32.4×10^{-6} and 237.5×10^{-6}, with a mean value of 110.9×10^{-6} (Fig. 3a) and $\sigma = 35.4 \times 10^{-6}$ These

values are typical for magnetic fabrics of mudrocks dominated by paramagnetic minerals (e.g., Tarling and Hrouda, 1993). They are consistent with those reported for the same rocks in the area by Pueyo-Anchuela et al. (2013), who confirmed the dominant paramagnetic character of these rocks on the basis of detailed rock magnetic analyses (90% in average). Our own rock magnetic results (e.g., thermomagnetic curves, Fig. 3c), show a hyperbolic decay of magnetic susceptibility from room temperature up to ~ 400 °C, which also indicates a dominant paramagnetic behaviour (Fig. 3c). Besides, the thermomagnetic runs also show sharp decays at 580 °C related to the presence of magnetite. Above this temperature and reaching up 680 °C, the remaining susceptibility experiences a final decay that indicates variable amounts of hematite. Thermomagnetic runs are not reversible, and cooling curves show a big increase of susceptibility at around 520–550°C related to the neoformation of magnetite upon heating (Fig. 3c).

The orientations of the axes of the magnetic fabrics in the Martes section are shown before and after bedding correction (Fig. 4). The k_{max} axes present low inclinations with a general WNW-ESE direction both before (Fig. 4a) and after bedding correction (Fig. 4b), which is broadly parallel to the bedding strike and the regional structural trend. The direction of the k_{max} axes after bedding correction slightly changes as a function of the stratigraphic position of the samples: k_{max} directions in the lower part of the section show values of around 290° (when plotted to the west) that shift, albeit gradually and displaying some variability, to a more E-W directed trend (e.g., 270°) towards the top of the section (Fig. 5d). Concerning the k_{min} axes, they display a slight girdle perpendicular to the average k_{max} before bedding correction (Fig. 4a), and cluster vertical after the variable bedding of the different strata (Fig. 4d) is corrected (Fig. 4b).

The different parameters of the AMS vary throughout the stratigraphic log (Fig. 5), the mean susceptibility (k_m) shows a decreasing trend upwards the section. Thus, mean susceptibility is slightly higher in the first 400 m of the section (average of 134.2×10^{-6}), relatively constant in the middle part of the section down to ~ 1600 m (average of 113.1×10^{-6}), and progressively decreases towards the top of the succession (average of 78.5×10^{-6}), after displaying a prominent peak ($\sim 200 \times 10^{-6}$) around 1670 m (Fig. 5a). The corrected degree of anisotropy (P') is overall higher (up to 1.2) in the first 400 m of the section and in the interval around 1670 m, and lower (typically < 1.1) within the rest of the section (Figs. 4c and 5b). The shape parameter (T) shows the predominance of oblate ellipsoids (average values of 0.5), although triaxial ($T \approx 0$) and prolate ($T < 0$) ellipsoids are frequent throughout the section, especially in the lower and upper thirds of the sequence (Figs. 4c and 5c). The three parameters (k_m, P' and T) exhibit a slight correlation (Fig. 4c), with $P' > 1.05$ typically corresponding to samples that have high k_m and oblate ellipsoids with $T > 0.5$.

4.2 Paleomagnetism

The NRM intensity of the studied samples ranges from 118.78×10^{-6} to 4964.72×10^{-6} A m^{-1}, with an average of 1044.95×10^{-6} A m^{-1} and $\sigma = 798.36 \times 10–^{6}$ A m^{-1} (Fig. 3b). After stepwise demagnetization of the NRM, three

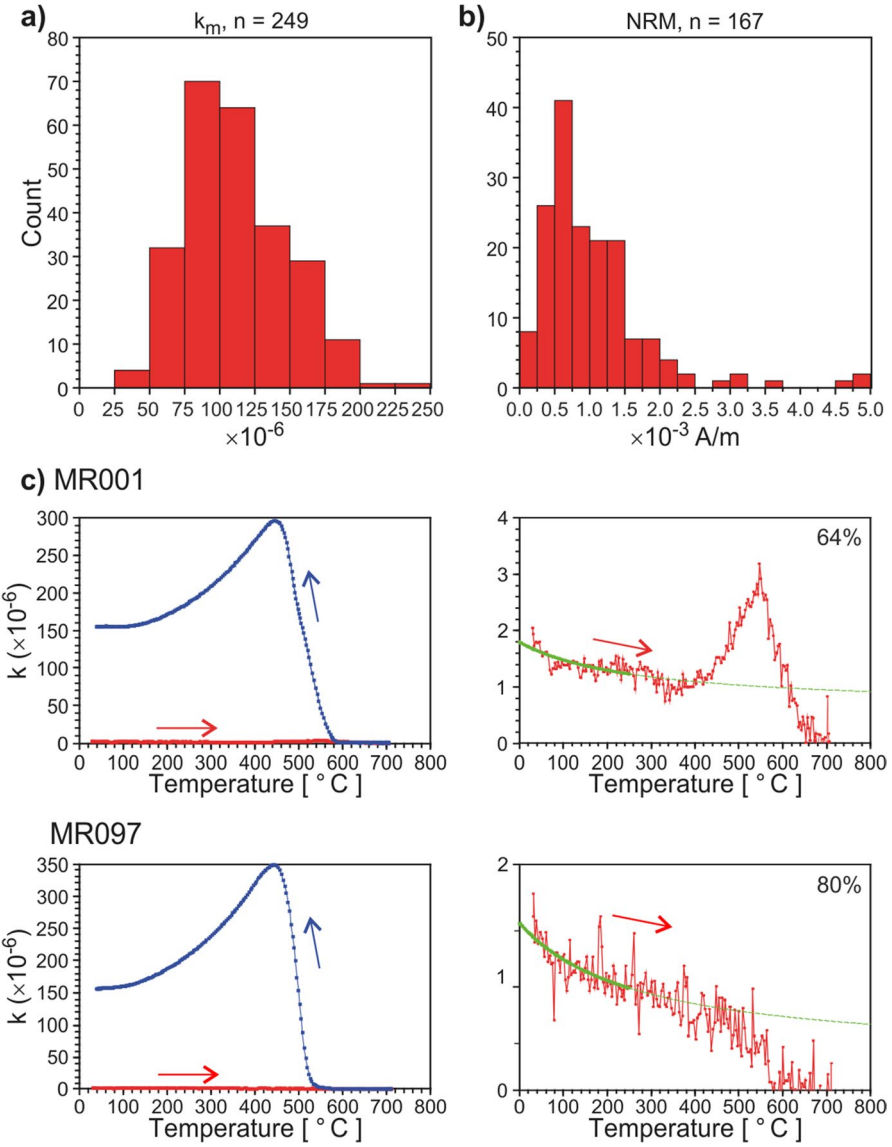

Fig. 3 Histogram of **a)** the mean magnetic susceptibility (k_m) and **b)** natural remanent magnetization (NRM); **c)** temperature dependence of bulk magnetic susceptibility k of two representative samples. Hyperbolic paramagnetic fitting of the heating curve (Hrouda et al., 1997) and the resulting percentage of the paramagnetic fraction is shown on the right hand side

components can be isolated in most of the samples. A low temperature component demagnetized between 100–150°C and 250–300°C, with northern directions and positive inclinations before bedding correction, is interpreted as a present-day field overprint and will not be further considered. Above 540–570°C and up to

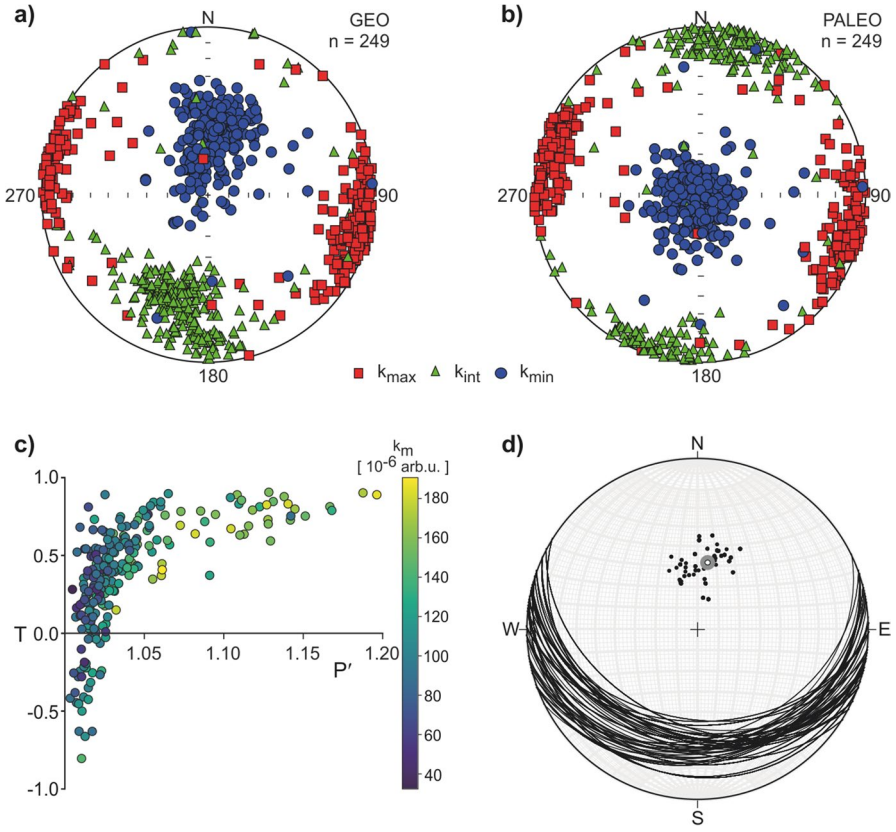

Fig. 4 Scalar parameters and orientation of the axes of the measured magnetic fabrics. Equal area projection of the magnetic susceptibility ellipsoid axes of all measured specimens: **a)** before bedding correction; **b)** after bedding correction; **c)** plot of shape parameter (*T*) versus corrected degree of anisotropy (*P′*), with color-coded mean susceptibility; **d)** equal area projection of bedding planes and poles (black dots) and mean bedding pole (blank circle) with α_{95} confidence angle (grey circle)

650–680°C, a paleomagnetic component likely carried by hematite is identified in most of the studied samples (Fig. 6b–d). This paleomagnetic component displays either northerly directions with positive inclinations or southerly directions with negative inclinations after bedding correction. It is consistent with a primary magnetization, according to the fold tests conducted in the area by previous authors (Oliva-Urcia et al., 2012, 2019; Pueyo-Anchuela et al., 2012; Anastasio et al., 2020; Pueyo et al., 2022), and is considered in this work as the ChRM. From the 167 demagnetized samples, the ChRM has been isolated and calculated in 163 samples; once the quality filters have been applied, 100 directions (~60% of the samples) remain for the calculation of average discretized paleomagnetic directions. Besides, from 250–300°C to 500–570°C, an additional component likely carried by magnetite is identified in 137 samples (Fig. 6a), typically displaying southerly directions and negative inclinations after bedding correction. Our working hypothesis is that

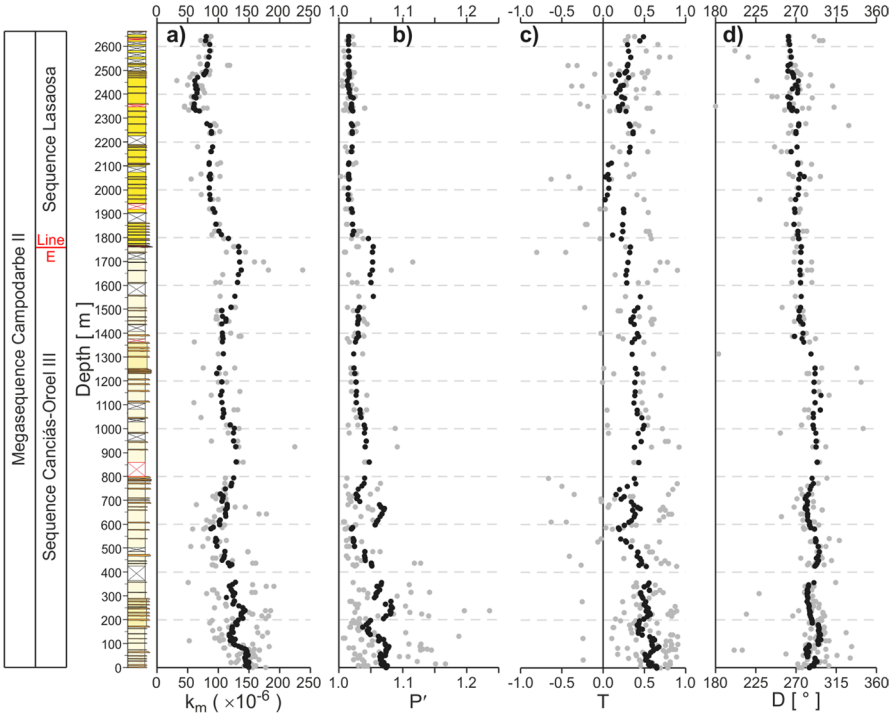

Fig. 5 Anisotropy of magnetic susceptibility results of the Martes section plotted as a function of stratigraphic position, with individual data in grey and running averages (9 sites window) in black. **a)** Mean susceptibility k_m; **b)** corrected degree of anisotropy P'; **c)** shape parameter T; and **d)** declination D of the maximum susceptibility axes k_{max} after bedding correction (shown along its westward projection)

this component might represent a secondary magnetization acquired before folding by pedogenetic processes, and will not be considered further.

5 Discussion

5.1 Significance of the magnetic fabrics of the Campodarbe Formation

The mudrocks from the Campodarbe Formation studied here share all the characteristics, both in terms of scalar parameters and in the directional properties of the ellipsoids, of those classically attributed to Type IIa magnetic fabrics (Parés, 2015). Thus, they show the clear imprint of the first stages of compressive deformation over-imposed on an initial sedimentary fabric. In this early deformation stage, the phyllosilicates that constitute most of the bulk of the rock matrix become rotated in response to early LPS, and the fabrics behave as passive markers upon later deformation (Sagnotti et al., 1998; Parés et al., 1999; Parés, 2004, 2015; Cifelli et al.,

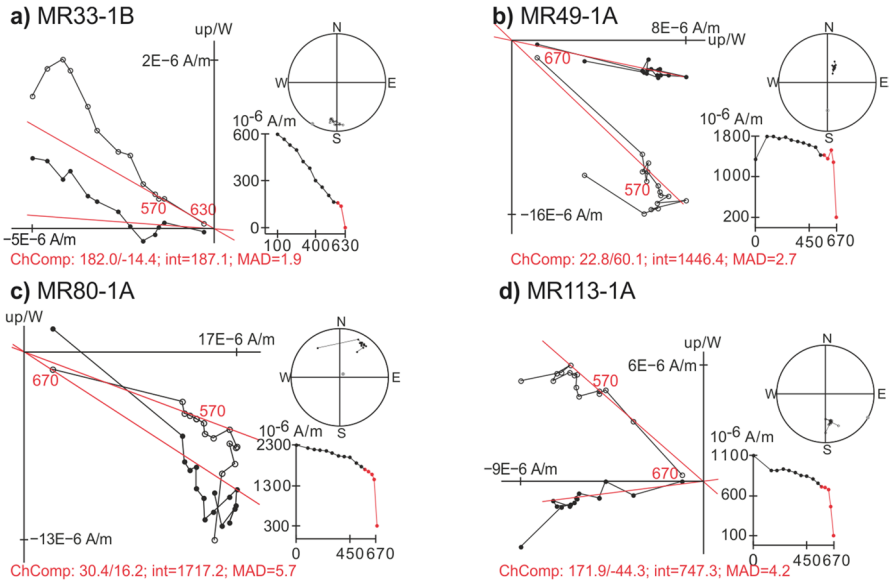

Fig. 6 Zijderveld (1967) plots of NRM intensity decay of representative samples, their thermal demagnetization and stereographic projection after bedding correction. ChComp shows declination/inclination of ChRM, its intensity, and maximum angular deviation

2004; Weaver et al., 2004; Larrasoaña et al., 2004, 2011; Soto et al., 2009; Pueyo-Anchuela et al., 2012, 2013; Pocoví et al., 2014; Sierra-Campos et al., 2025a). Given the Priabonian-Rupelian age of the studied rocks and their geological context (Hogan and Burbank, 1996; Oliva-Urcia et al., 2019), we interpret that the tectonic magnetic fabrics were locked in under the imprint of the LPS in the foreland of the basement thrust system deforming the northern Jaca-Pamplona Basin (which includes the Gavarnie thrust system). In this context, it is tempting to interpret the variability observed in the scalar parameters of the studied rocks along the Martes section (Fig. 5) in terms of variable intensities of LPS. Yet, the slight correlation observed between k_m and the evolution of P' and T along the section, with overall larger values in the lowermost 400 m of the succession (Fig. 5), suggest that at least part of this variability might be driven by changes in the relative fraction between phyllosilicate grains and the carbonate and/or the ferromagnetic s.l. content.

Regardless, what is most remarkable about the AMS of the studied rocks is the evolution of the discretized, average k_{max} directions as a function of the stratigraphic (and hence temporal) position of the samples. As previously described, these k_{max} directions shift from values of ~ 290° in the lower part of the succession (e.g., 35.8 Ma) to ~ 270° towards its upper part (33.4 Ma, numerical ages following Hogan and Burbank, 1996; Oliva-Urcia et al., 2019) (Table 1, Figs. 7, 8 and 9b). Although the errors associated to these average values are large and comparable in magnitude to the directional variation they record (~ 20°, Jelínek, 1978, ~ 15°–25°), the systematic shift observed in the orientation of the discretized k_{max} directions suggests that

they might record either a change in the direction of LPS or the rotational kinematics of the studied succession. The paleomagnetic results obtained for the same succession are paramount to discern between these two possibilities, since they enable to independently quantify the VARs undergone by the studied rocks. Thus, the angular deviation observed between the average declination of the discretized paleomagnetic results and the Eocene reference direction for the area (Pedrera et al., 2023) points to variable VAR magnitudes along the succession (Table 2 and Fig. 8), with VARs of around + 6° and + 12° (clockwise) in the lower part of the section and VARs of –7° and –14° (counterclockwise) towards its top (Fig. 9a). As it happens with the orientation of the magnetic ellipsoids, the errors associated to the mean paleomagnetic directions (ΔD) are large (20°–30°) and comparable in magnitude to the variability of the rotation they record (Table 2). Yet, paleomagnetic directions show a systematic change along the section that involves a differential rotation of nearly 30° from its base to its top (Fig. 9a). Noticeably, the differential rotation recorded by the paleomagnetic data is entirely consistent with the differential rotation that can be inferred from the declination of the $k_{\max}$ in magnetic ellipsoids (Fig. 9b), so that they display a clear linear correlation when plotted against each other (Fig. 9c). This correlation supports the idea that magnetic fabrics of Type IIa behave as passive markers upon subsequent deformation, and validate their use to quantify VARs as has been demonstrated in previous studies (Sagnotti et al., 1998; Cifelli et al., 2004; Weaver et al., 2004; Pueyo Anchuela et al., 2012. Although the correlation found between the orientation of the magnetic ellipsoids and the paleomagnetic results seems clear and robust (Fig. 9c), it is important to note that the errors associated to both data sets preclude the delineation of statistically significant rotations (Tables 1 and 2, Fig. 9a,b). Based on these observations we interpret that our results from the Martes section are at the edge of the resolution of the AMS and paleomagnetic results. Still, we think that they can be used to provide useful insights into the kinematics of the study area, as we discuss in the following section.

Table 1 Anisotropy of magnetic susceptibility data of the Martes section; k_m: mean susceptibility; P': corrected degree of anisotropy; T: shape parameter. All these parameters are with its standard deviation. D: declination of the k_{max} axes; α_{95}: 95% confidence angle of k_{max}; N: Number of measured samples; Age: age of the site (Hogan and Burbank, 1996; Oliva-Urcia et al., 2019); Rot.: rotation of the k_{max} axes with respect to the MRs-7

Interval [m]	Site	k_m ($\times 10^{-6}$)	D [°]	α_{95}	P'	T	N	Age [Ma]	Rot
0–400	MRs-1	134.2 ± 31.5	283.5	32.4	1.065 ± 0.049	0.537 ± 0.267	84	35.8	10.90
400–800	MRs-2	106.3 ± 27.1	287.1	18.8	1.042 ± 0.056	0.322 ± 0.441	46	35.4	14.50
800–1200	MRs-3	119.2 ± 34.1	291.0	12.8	1.072 ± 0.107	0.466 ± 0.267	19	34.9	18.40
1200–1600	MRs-4	107.0 ± 18.8	277.9	11.2	1.028 ± 0.009	0.355 ± 0.259	20	34.6	5.30
1600–2000	MRs-5	116.3 ± 38.06	276.5	14.1	1.050 ± 0.079	0.277 ± 0.416	24	34.2	3.90
2000–2400	MRs-6	76.4 ± 18.5	271.4	22.7	1.018 ± 0.008	0.184 ± 0.299	29	33.7	–1.20
2400–2700	MRs-7	75.5 ± 17.6	272.6	13.1	1.015 ± 0.005	0.280 ± 0.333	27	33.4	0.00

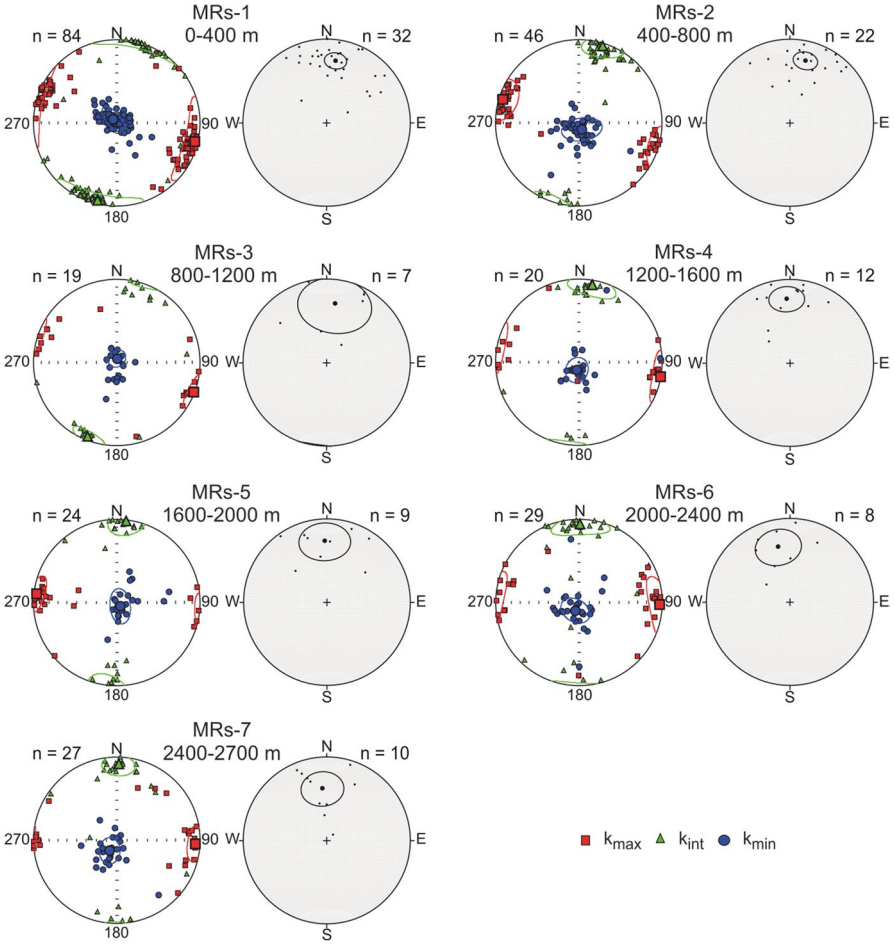

Fig. 7 Equal area projection after bedding correction of the magnetic fabrics of the studied sections (left plot of each pair) in comparison with the paleomagnetic directions (right plot of each pair)

5.2 Implications for unravelling the kinematics of the South Pyrenean Zone

The central part of the Jaca-Pamplona Basin, located south of the Leire thrust, represents a transition area where the clockwise VARs documented in the eastern part of the basin (Pueyo-Anchuela et al., 2012; Mochales et al., 2012; Rodríguez-Pintó et al., 2016; Pueyo et al., 2022) dampen towards the west (Larrasoaña et al., 2003; Oliva-Urcia et al., 2012; Sierra-Campos et al., 2025b; see compilation in Pedrera et al., 2023). In spite of the large dispersion inherent to our dataset and the fact that the reported rotations are not statistically significant, the average AMS and paleomagnetic results from the Martes section record a strikingly consistent, differential rotation of about 30º between its upper and its lower part. This variation along the profile can be interpreted as resulting from; i) an areal distinction between

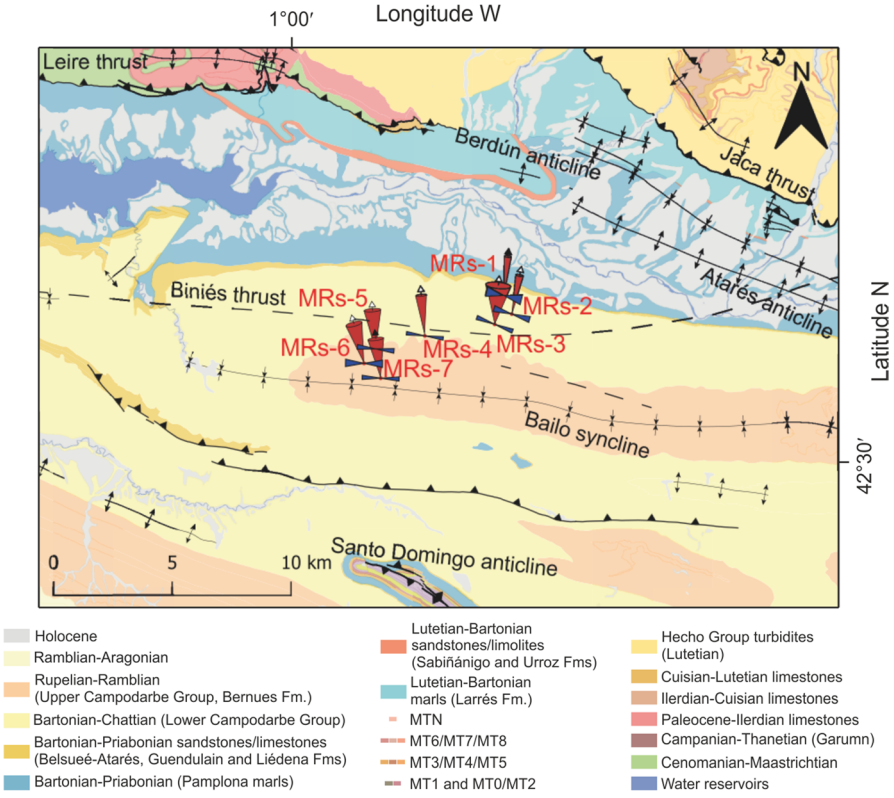

Fig. 8 Paleomagnetically-derived vertical axes rotations (VARs) and directions of the maximum susceptibility k_{max} shown along with the geological map of the of the studied area (modified from Robador Moreno et al., 2024a,b; Government of Navarre, 2024). The cones represent the VARs and the corresponding confidence angles

a north-eastern, clockwise-rotated portion of the section (MRs-1 to MRs-3) and a south-western, anticlockwise-rotated portion of the section (MRs-4 to MRs-7) or ii) a progressive rotation recorded through time. Data quality and scattering preclude discerning between these two options, but additional constraints from the regional paleomagnetic and structural knowledge can help discerning between them. In the first scenario, the studied area should be divided by a transition or transfer zone separating the two regional-scale rotation domains. The Martes section is located just 5–10 km north of the Santo Domingo anticline, which represents a detachment fold cored by a thick unit of Late-Middle Triassic evaporites (i.e., the Keuper evaporites). The shortening accommodated by this structure decreases westwards with the anticline ending laterally along a pericline that crops out to the south of the sampled sequence (Fig. 8) (Pueyo et al., 2021, 2025). The lateral termination of the anticline overlaps a transition between a negative gravity anomaly in the east and a positive one in the west which indicates a significant westward thinning of the Late-Middle Triassic evaporites representing the main décollement in the area

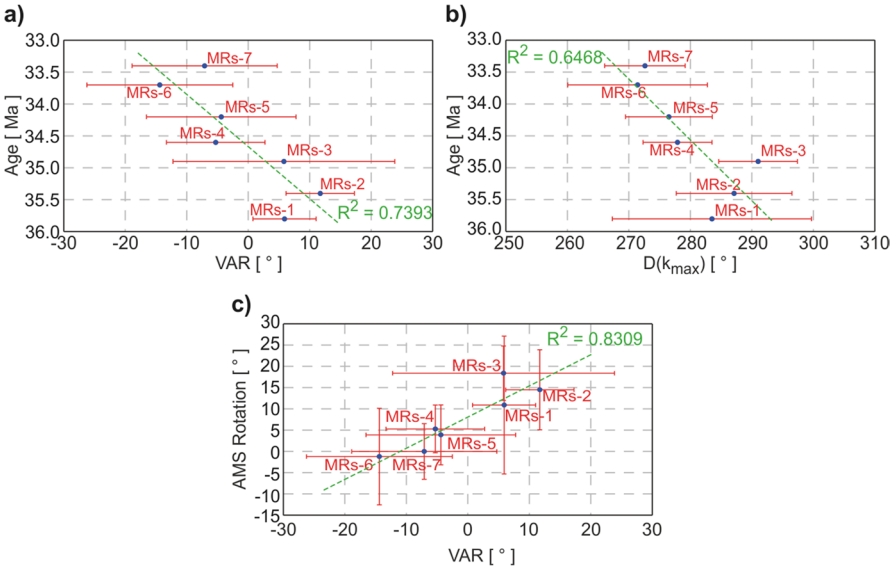

Fig. 9 Age of the site as a function of the **a)** vertical axes rotation (VAR), and **b)** declination D of the direction of maximum susceptibility k_{max}; **c)** anisotropy of magnetic susceptibility rotation in dependence of VAR; R^2 represents goodness of the linear fit

(Calvín et al., 2018; Pueyo et al., 2025). Besides, the lateral termination of the Triassic-cored anticline aligns northwards with the prominent NE-SW-trending basement anticline hangingwall of the Biniés thrust (Muñoz et al., 2025). They together define a diffuse, oblique zone where basement thrusts in the footwall of Biniés (Jaca thrust system) end laterally (Fig. 8), this supporting the notion that the study area could represent the pining point of the VAR undergone by the eastern part of the Jaca-Pamplona Basin (as interpreted for the Santo Domingo pericline further south; Oliva-Urcia et al., 2012; Pueyo-Anchuela et al., 2012; Calvín et al., 2018). In this context, clockwise rotations in the lower part of the Martes section could result from differential shortening in the Biniés basement thrust, this localizing in the area where its hangingwall cutoff changes strike and becomes oblique. Additionally, the lateral termination across the area of a basement thrust from the Jaca thrust system (footwall of Biniés) can also provoke clockwise rotations in its hangingwall (where sites MRs-1 to MRs-3 are located; Fig. 8) which could concur with rotations derived from the thickness decrease of Late-Middle Triassic evaporites to the west of the Santo Domingo anticline. The Biniés basement thrust and the Jaca thrust system were active during Oligocene–Miocene times (Muñoz et al., 2025), which implies that related rotations should also have an Oligocene–Miocene age, having occurred after deposition of the mudrocks from the Martes section.

In the second hypothesized scenario (i.e., progressive rotation through time), given the age of the sampled sequence, the combination of our AMS and paleomagnetic results suggest that clockwise rotations occurred from ~ 36 Ma (Middle Priabonian, Table 2) and were completed at 34.6 Ma (Late Priabonian, Table 2), largely

Table 2 Paleomagnetic rotations in the Martes section; *n*: number of measured samples; DD: dip direction; *N*: number of considered samples; *NRM*: natural remanent magnetization; σ: standard deviation; *D*: declination after bedding correction; *I*: inclination after bedding correction; ΔD: confidence angle (Demarest, 1983); α_{95}, κ and *R*: Fisher (1953) statistics parameters; *VAR*: vertical axis rotation; ΔR *VAR*: confidence angle of the VAR

Interval [m]	Site	*n*	Lat. [°N]	Long. [°E]	Strike [°]	Dip [°]	DD	*N*	*NRM* ± σ [10^{-6} A/m]	*D* [°]	*I* [°]	α_{95} [°]	ΔD [°]	κ	*R*	Age [Ma]	VAR [°]	ΔR *VAR* [°]
0–400	MRs-1	47	42.562	–0.8907	107.0	36.6	S	32	1160.1 ± 647.9	8.2	26.3	9.2	10.3	8.6	0.887	35.8	5.9	10.7
400–800	MRs-2	30	42.555	–0.8867	99.5	42.7	S	22	995.3 ± 594.9	14.0	24.6	10.1	11.1	9.5	0.899	35.4	11.7	11.5
800–1200	MRs-3	13	42.551	–0.8955	88.0	34.1	S	7	1051.6 ± 726.6	8.1	29.5	31.4	36.1	4.0	0.815	34.9	5.8	36.2
1200–1600	MRs-4	14	42.547	–0.9312	83.4	32.3	S	12	618.3 ± 250.7	357.0	24.3	14.6	16.0	9.0	0.907	34.6	–5.3	16.3
1600–2000	MRs-5	15	42.542	–0.9563	73.8	25.6	S	9	1183.2 ± 1434.4	357.9	27.4	21.6	24.3	5.9	0.865	34.2	–4.4	24.5
2000–2400	MRs-6	24	42.537	–0.9622	101.0	24.3	S	8	1060.1 ± 1126.0	347.9	33.0	19.9	24.0	7.6	0.899	33.7	–14.4	24.2
2400–2700	MRs-7	20	42.531	–0.9537	104.2	17.0	S	10	1105.4 ± 533.0	355.2	37.6	18.7	23.6	6.9	0.882	33.4	7.1	23.8

before deposition of the top units in the Martes section, which are earliest Rupelian according to the magnetostratigraphic results provided for Hogan and Burbank (1996) and Oliva-Urcia et al. (2019). This is consistent with the geological inferences made on the age of the VAR undergone by oblique folds in the eastern part of the Jaca-Pamplona basin (Pueyo et al., 2002, 2022; Mochales et al., 2012; Muñoz et al., 2013; Rodríguez-Pintó et al., 2016). However, a Priabonian rotation age is grossly inconsistent with the Oligocene, clockwise rotations recorded by remagnetized components in the Internal Sierras and the northern and central part of the Jaca-Pamplona Basin (Oliva-Urcia and Pueyo, 2007; Izquierdo-Llavall et al., 2015; Pueyo et al., 2024). These rotations in remagnetized components generally range between 10° and 20°, with values that are in the range of those defined in the lower part of the Martes (this work) and Berdún sections (see location in Fig. 2; Sierra-Campos et al., 2025b). If clockwise rotations are considered as Priabonian in age, they should take place coevally to thrusting along the Gavarnie thrust system, to the north of the study area. Around 20 km to the east of the Martes section, the Gavarnie basement thrust system is interpreted to be disconnected from the thrust front at the External Sierras (to the south of the study area) (Muñoz et al., 2025). This results from the lack of Late-Middle Triassic evaporites beneath the northern Jaca-Pamplona Basin and provides a structural configuration at Priabonian times where the N-S transfer of shortening gradients and rotations from the Gavarnie thrust system to the study area was locked.

In addition to these tectonic inferences made on the basis of our AMS and paleomagnetic results, our paleomagnetic results alone provide additional constraints to quantify rotations in the studied part of the South Pyrenean Zone (SPZ). Thus, paleomagnetic results point to a clockwise VAR of around 6° and 12°in the lower part of the section and a counterclockwise VAR of 7° and 14° in its upper part (Fig. 9a). Although the errors associated to these rotations are comparable with the magnitude of the rotations themselves, it is remarkable that such variable VARs can be only reconciled with the progressive clockwise rotation hypothesis if a later (Oligocene) counterclockwise rotation of 7°–14° is considered. Such a later counterclockwise rotation can be associated with Oligocene thrusting along the Serrablo or Biniés basement thrusts or the Jaca basement thrust system (following the nomenclature in Muñoz et al., 2025). Conversely to the Gavarnie thrust system, these basement structures connect to Late-Middle Triassic evaporites around 20 km to the east of the Martes section and transferred the shortening to the thrust front at the External Sierras from Early Oligocene times (Muñoz et al., 2025). Although the interpretation of magnetic data requires a careful integration with structural constraints, the results presented in this work further validate the combined use of AMS and paleomagnetic results to unravel the kinematics of thrust units in orogenic belts. In the study case, the integration of magnetic results within the regional geology framework could favour the hypothesis of the spatial over the temporal variability of the studied rotations. However, we should be cautious and wait for the outcome of ongoing studies on the tectonic evolution of the area (*Izquierdo-Llavall* et al.*, unpublished data*) before one of the two hypotheses presented here can be confidently favoured.

6 Conclusions

A combined AMS and paleomagnetic study along a stratigraphic section composed by the continental materials of the Campodarbe Formation (Priabonian-Rupelian times) in the Jaca-Pamplona Basin, southern Pyrenees, was carried out. This study allows us to gain insights on the tectonic evolution of the central part of this basin. The AMS reflects the imprint of the first stages of compressive deformation for it was locked-in under the effects of the LPS during the early diagenesis, in the foreland of the basement thrust system deforming the northern Jaca-Pamplona Basin. The AMS shows a dominance of oblate ellipsoids and the k_{max} axes display an overall WNW-ESE direction, within the bedding plane and parallel to the main structures in the area. Those magnetic fabrics are classified as Type IIa and show k_{max} directions around 290° in the lower part of the section, that change progressively towards the top of the section to a direction around 270°. Paleomagnetically-derived VARs registered in the lower part of the section show a clockwise rotation of about 6° to 12° whereas the upper part of the section records a counterclockwise rotation of around 7° to 14°. Both AMS and paleomagnetism register a differential rotation of about 25° along the section, where the AMS behave as passive marker of the deformation and supports the use of AMS to quantify VARs occurred after magnetic fabrics are locked in.

The along-section change in VARs are analysed under two different hypotheses that consider either a spatial versus temporal change in the rotations. These differential rotations could result from lateral changes in the Biniés basement thrust or the Jaca thrust system that were active during Oligocene times (i.e., later than the depositional age of the Martes section) or, alternatively, be related to the spatial distribution of the studied sites with respect to the main structures present in the area. In any case, our contribution highlights the extraordinary sensitivity that magnetic fabrics have to pinpoint tectonic processes, spurring the relevance they have, and will continue to have, on furnishing our understanding of the tectonic evolution of fold-and-thrust-belts and foreland basins.

7 Supplementary Data

Supplementary data, containing the AMS data, including the raw data, are available at: https://doi.org/10.5281/zenodo.16811474.

Supplementary Information The online version contains supplementary material available at https://doi.org/10.1007/s11200-026-00018-5.

Acknowledgements This study was funded by project UKRIA-4D (PID2019-104693GB-I00) of the Spanish Ministry of Science and Innovation ("ERDF A way of making Europe"), which also covered the predoctoral contract of P. Sierra-Campos (PRE2020-092425), and also by the project KINETRANS (PID2024-157800NB-C21), also from the Spanish Ministry of Science and Innovation.

Author contributions **P. Sierra-Campos:** Writing – original draft, Writing – review and editing, Visualization, Validation, Supervision, Software, Methodology, Investigation, Formal analysis, Data curation, Conceptualization. **P. Calvín:** Writing – review and editing, Visualization, Validation, Supervision, Software, Methodology, Investigation, Formal analysis, Data curation, Conceptualization. **E. Izquierdo-Llavall:** Writing – review and editing, Validation, Methodology, Investigation. **M. Montes:** Writing – review and editing, Validation, Methodology, Investigation. **A. Luzón:** Writing – review and editing, Validation, Methodology, Investigation. **E. Bellido:** Writing – review and editing, Investigation. **E. Beamud:** Writing – review and editing, Supervision, Data curation. **E.L. Pueyo:** Writing – review and editing, Visualization, Validation, Supervision, Software, Resources, Project administration, Funding acquisition, Methodology, Investigation, Formal analysis, Data curation, Conceptualization. **J.C. Larrasoaña:** Writing – original draft, Writing – review and editing, Visualization, Validation, Supervision, Software, Resources, Project administration, Funding acquisition, Methodology, Investigation, Formal analysis, Data curation, Conceptualization.

Funding Open Access funding provided thanks to the CRUE-CSIC agreement with Springer Nature.

Data availability The authors declare that the data supporting the findings of this study are available within the paper, its supplementary information files, and the Zenodo repository (https://doi.org/10.5281/zenodo.16811474).

References

Allerton S., 1998. Geometry and kinematics of vertical-axis rotations in fold and thrust belts. *Tectonophysics*, **299**, 15–30., https://doi.org/10.1016/S0040-1951(98)00196-6

Allmendinger R.W., Cardozo N.C. and Fisher D., 2013. *Structural Geology Algorithms: Vectors & Tensors*. Cambridge, Cambridge University Press, Cambridge, U.K., 289pp.

Anastasio D.J., Teletzke A.L., Kodama K.P., Parés J.M. and Gunderson K.L., 2020. Geologic evolution of the Peña flexure, Southwestern Pyrenees mountain front, Spain. *J. Struct. Geol*., **131**, Art. No.103969, https://doi.org/10.1016/j.jsg.2019.103969

Boiron T., Aubourg C., Grignard P.A. and Callot J.P., 2020. The clay fabric of shales is a strain gauge. *J. Struct. Geol*., **138**, Art.No.104130, https://doi.org/10.1016/j.jsg.2020.104130

Borradaile G.J. and Henry B., 1997. Tectonic applications of magnetic susceptibility and its anisotropy. *Earth Sci. Rev*., **42**, 49–93, https://doi.org/10.1016/S0012-8252(96)00044-X

Borradaile G.J. and Jackson M., 2004. Anisotropy of magnetic susceptibility (AMS): magnetic petrofabrics of deformed rocks. In: Martín-Hernández F., Lüneburg C.M., Aubourg C. and Jackson M. (Eds), *Magnetic Fabric, Methods and Applications*. *Geol. Soc. London Spec. Publ.*, **238**, 299–360, https://doi.org/10.1144/GSL.SP.2004.238.01.18

Borradaile G.J. and Jackson M., 2010. Structural geology, petrofabrics and magnetic fabrics (AMS, AARM, AIRM). *J. Struct. Geol*., **32**, 1519–1551, https://doi.org/10.1016/j.jsg.2009.09.006

Borradaile G.J., 2001. Magnetic fabrics and petrofabrics: Their orientation distributions and anisotropies. *J. Struct. Geol*., **23**, 1581–1596, https://doi.org/10.1016/S0191-8141(01)00019-0

Calvín P., Santolaria P., Casas A.M. and Pueyo E.L., 2018. Detachment fold vs. ramp anticline: a gravity survey in the southern Pyrenean front (External Sierras). *Geol. J.*, **53**, 178–190, https://doi.org/10.1002/gj.2884

Cámara P. and Klimowitz J., 1985. Interpretación geodinámica de la vertiente centro-occidental surpirenaica (Cuencas de Jaca-Tremp). *Estudios Geológicos*, **41**, 391–404, https://doi.org/10.3989/egeol.85415-6720

Chadima M. and Hrouda F., 2012. *Cureval 8.0: Thermomagnetic Curve Browser for Windows*. AGICO Inc., Brno, Czechia

Chadima M., Hrouda F., Ježek J. and Jelínek V., 2024. *Anisotropy Data Browser for Windows*. AGICO Inc., Brno, Czechia

Choukroune P., 1992. Tectonic evolution of the Pyrenees. *Annu. Rev. Earth Planet. Sci.,* **20**, 143–158, https://doi.org/10.1146/annurev.ea.20.050192.001043

Cifelli F., Rossetti F., Mattei M., Hirt A.M., Funiciello R. and Tortorici L., 2004. An AMS, structural and paleomagnetic study of Quaternary deformation in eastern Sicily. *J. Struct. Geol*., **26**, 29–46, https://doi.org/10.1016/S0191-8141(03)00092-0

Costa E., Garcés M., López-Blanco M., Beamud E., Gómez-Paccard M. and Larrasoaña J.C., 2010. Closing and continentalization of the South Pyrenean foreland basin (NE Spain): Magnetochronological constraints. *Basin Res*., **22**, 904–917, https://doi.org/10.1111/j.1365-2117.2009.00452.x

Demarest H.H., 1983. Error analysis for the determination of tectonic rotation from paleomagnetic data. *J. Geophys. Res*., **88**, 4321–4328, https://doi.org/10.1029/JB088iB05p04321

Dreyer T., Corregidor J., Arbués P. and Puigdefábregas C. 1999. Architecture of the tectonically influenced Sobrarbe deltaic complex in the Ainsa Basin, northern Spain. *Sediment. Geol.,* **127**, 127–169, https://doi.org/10.1016/S0037-0738(99)00056-1

Fisher R.A., 1953. Dispersion on a sphere. *Proc. R. Soc. London A*, **217**, 295–305

Garcés M., López-Blanco M., Valero L., Beamud E., Muñoz J.A., Oliva-Urcia B., Vinyoles A., Arbués P., Cabello P. and Cabrera L., 2020. Paleogeographic and sedimentary evolution of the South Pyrenean foreland basin. *Mar. Pet. Geol*., **113**, Art.No.104105, https://doi.org/10.1016/j.marpetgeo.2019.104105

Government of Navarre, 2024. Mapa geológico digital continuo 1:25000, [enV línea] Navarra, Gobierno de Navarra. Información geográfica propiedad del Gobierno de Navarra https://idena.navarra.es/navegar/#ZXh0fGJhc2V8bWFwYWJhc2V8bGF5ZXJzfHV8Ly9pZGVuYS5uYXZhcnJhLmVzL29nYy93bXN8bnxnZW9sb2dpYXxvfHZ8aHx1cnxmfHR8SURFTkF8aXxsY2F0LTEtMV4xXjYwNzYxNS4yNzV8NDcwNjU1NS4zNzZ8NjY5MDU1LjI3NXw0NzM0MzU1LjM3Nl4kMHxASXxKfEt8TF18MXwyfDN8QCQ0fDV8Nnw3fDh8SHw5fC0xfEF8LTF8QnwtNXxDfC01fER8RXxGfEddXV0=

Gracia-Puzo F., Aubourg C. and Casas-Sainz A., 2021. A fast way to estimate the clay fabric from shale fragments. Key example from a strained thrust footwall (Pyrenees). *J. Struct. Geol.,* **152**, Art. No.104443, https://doi.org/10.1016/j.jsg.2021.104443

Graham J.W., 1954. Magnetic susceptibility anisotropy, an unexploited petrofabric element. *Geol. Soc. Am. Bull*., **65**, 1257–1258

Hirt A.M., Lowrie W., Luneburg C., Lebit H. and Engelder T., 2004. Magnetic and mineral fabric development in the Ordovician Martinsburg Formation in the Central Appalachian fold and thrust belt, Pennsylvania. In: Martıín-Hernández F., Lüneburg C.M., Aubourg C. and Jackson M. (Eds), *Magnetic Fabric, Methods and Applications*. *Geol. Soc. London Spec. Publ*., **238**, 109–126, https://doi.org/10.1144/GSL.SP.2004.238.01.09

Ho N.C., Peacor D.R. and van der Pluijm B.A., 1995. Reorientation mechanisms of phyllosilicates in the mudstone-to-slate transition at Lehigh Gap, Pennsylvania. *J. Struct. Geol.*, **17**, 345–356, https://doi.org/10.1016/0191-8141(94)00065-8

Hogan P.J. and Burbank D.W., 1996. Evolution of the Jaca piggyback basin and emergence of the External Sierra, southern Pyrenees. In: Friend P.F. and Dabrio C.J. (Eds), *Tertiary Basins of Spain*, 153–160. Cambridge University Press, Cambridge, U.K.

Hrouda F. and Janák F., 1976. The changes in shape of the magnetic susceptibility ellipsoid during progressive metamorphism and deformation. *Tectonophysics*, **34**, 135–148, https://doi.org/10.1016/0040-1951(76)90181-5

Hrouda F. and Kahan S., 1991. The magnetic fabric relationship between sedimentary and basement nappes in the High Tatra Mountains, N. Slovakia. *J. Struct. Geol*., **13**, 432–442, https://doi.org/10.1016/0191-8141(91)90016-C

Hrouda F., Jelínek V. and Zapletal K., 1997. Refined technique for susceptibility resolution into ferromagnetic and paramagnetic components based on susceptibility temperature variation measurement. *Geophys. J. Int*., **129**, 715–719, https://doi.org/10.1111/j.1365-246X.1997.tb04506.x

Hrouda F., 1979. Strain interpretation of magnetic anisotropy in rocks of the Nízký Jeseník Mountains (Czechoslovakia). *Sborník Geologických Věd.*, **16**, 27–62

Hrouda F., 1982. Magnetic anisotropy of rocks and its application in geology and geophysics. *Geophys. Surv.*, **5**, 37–82, https://doi.org/10.1007/BF01450244

Izquierdo-Llavall E., Aldega L., Cantarelli V., Corrado S., Gil-Peña I., Invernizzi C. and Casas A.M., 2013. On the origin of cleavage in the Central Pyrenees: Structural and paleo-thermal study. *Tectonophysics*, **608**, 303–318, https://doi.org/10.1016/j.tecto.2013.09.027

Izquierdo-Llavall E., Sainz A.C., Oliva-Urcia B., Burmester R., Pueyo E.L. and Housen B., 2015. Multiepisodic remagnetization related to deformation in the Pyrenean Internal Sierras. *Geophys. J. Int.*, **201**, 891–914, https://doi.org/10.1093/gji/ggv042

Jelínek V., 1978. Statistical processing of anisotropy of magnetic susceptibility measured on groups of specimens. *Stud. Geophys. Geod.,* **22**, 50–62, https://doi.org/10.1007/BF01613632

Jelínek V., 1981. Characterization of the magnetic fabric of rocks. *Tectonophysics*, **79**, T63–T67, https://doi.org/10.1016/0040-1951(81)90110-4

Kirschvink J.L., 1980. The least-squares line and plane and the analysis of palaeomagnetic data. *Geophys. J. Int*., **62**, 699–718, https://doi.org/10.1111/j.1365-246X.1980.tb02601.x

Labaume P. and Teixell A., 2018. 3D structure of subsurface thrusts in the eastern Jaca Basin, southern Pyrenees. *Geol. Acta*, **16**, 477–498, https://doi.org/10.1344/GeologicaActa2018.16.4.9

Labaume P., Séguret M. and Seyve C., 1985. Evolution of a turbiditic foreland basin and analogy with an accretionary prism: Example of the Eocene south-Pyrenean basin. *Tectonics*, **4**, 661–685, https://doi.org/10.1029/TC004i007p00661

Labaume P., Meresse F., Jolivet M., Teixell A. and Lahfid A., 2016. Tectonothermal history of an exhumed thrust-sheet-top basin: An example from the south Pyrenean thrust belt. *Tectonics*, **35**, 1280–1313, https://doi.org/10.1002/2016TC004192

Larrasoaña J.C., Parés J.M., Millán H., del Valle J. and Pueyo E.L., 2003. Paleomagnetic, structural, and stratigraphic constraints on transverse fault kinematics during basin inversion: The Pamplona Fault (Pyrenees, north Spain). *Tectonics*, **22**, Art.o.1071, https://doi.org/10.1029/2002TC001446

Larrasoaña J.C., Pueyo E.L. and Parés J.M., 2004. An integrated AMS, structural, palaeo and rockmagnetic study of the Eocene marine marls from the Jaca-Pamplona basin (Pyrenees, N Spain): new insights into the timing of magnetic fabric acquisition in weakly deformed mudrocks. In: Martín-Hernández F., Lüneburg C.M., Aubourg C. and Jackson M. (Eds), *Magnetic Fabric, Methods and Applications*. *Geol. Soc. London Spec. Publ*., **238**, 127–144, https://doi.org/10.1144/GSL.SP.2004.238.01.10

Larrasoaña J.C., Gómez-Paccard M., Giralt S. and Roberts A.P., 2011. Rapid locking of tectonic magnetic fabrics in weakly deformed mudrocks. *Tectonophysics*, **507**, 16–25, https://doi.org/10.1016/j.tecto.2011.05.003

Martín-Hernández F. and Hirt A.M., 2003. The anisotropy of magnetic susceptibility in biotite, muscovite and chlorite single crystals. *Tectonophysics*, **367**, 13–28, https://doi.org/10.1016/S0040-1951(03)00127-6

McCaig A.M. and McClelland E., 1992. Palaeomagnetic techniques applied to thrust belts. In: McClay K.R. (Ed.), *Thrust Tectonics*, 209–216. Chapman and Hall, London, U.K.

Menzer R.L., Bonnel C., Gracia-Puzo F. and Aubourg C., 2024. Matrix deformation of marls in a foreland fold-and-thrust belt: The example of the eastern Jaca basin, southern Pyrenees. *J. Struct. Geol.*, **182**, Art.No.105114, https://doi.org/10.1016/j.jsg.2024.105114

Millán G.H., Pocoví J.A. and Casas Sainz A.M., 1995. El frente de cabalgamiento surpirenaico en el extremo occidental de las Sierras Exteriores. *Rev. Soc. Geol. Esp.*, **8**, 73–90 (in Spanish)

Millán Garrido H., Pueyo Morer E.L., Aurell Cardona M., Luzón Aguado A., Oliva-Urcia B., Martínez-Peña M.B. and Pocoví Juan A., 2000. Actividad tectónica registrada en los depósitos terciarios del frente meriodinal del Pirineo Central. *Rev. Soc. Geol. Esp*., **13**, 279–300 (in Spanish)

Millán G.H., 1996. *Estructura y cinemática del frente de cabalgamiento surpirenaico en las Sierras Exteriores Aragonesas*. Ph.D. Thesis. Universidad de Zaragoza, Zaragoza, pain (in Spanish)

Mochales T., Casas A.M., Pueyo E.L. and Barnolas A., 2012. Rotational velocity for oblique structures (Boltaña anticline, Southern Pyrenees). *J. Struct. Geol*., **35**, 2–16,https://doi.org/10.1016/j.jsg.2011.11.009

Mochales T., Pueyo E.L., Casas A.M. and Barnolas A., 2016. Restoring paleomagnetic data in complex superposed folding settings: The Boltaña anticline (Southern Pyrenees). *Tectonophysics*, **671**, 281–298, https://doi.org/10.1016/j.tecto.2016.01.008

Montes M.J., 2009. *Estratigrafía del Eoceno-Oligoceno de la cuenca de Jaca. Sinclinorio del Guarga*. Ph.D. Thesis. Universidad Barcelona, Barcelona, Spain (in Spanish)

Muñoz J.A., Beamud E., Fernández O., Arbués P., Dinarès-Turell J. and Poblet J., 2013. The Ainsa Fold and thrust oblique zone of the central Pyrenees: Kinematics of a curved contractional system from paleomagnetic and structural data. *Tectonics*, **32**, 1142–1175, https://doi.org/10.1002/tect.20070

Muñoz J.A., Izquierdo-Llavall E., Santolaria P., Toro R., Pueyo E. L., Casas A.M. and Granado P., 2025. Inheritance in shortening transfer and kinematics in fold-and-thrust belts: Revisiting the structure of

the Jaca Basin, Southern Pyrenees. *Earth Sci. Rev.*, **270**, Art.No.105237, https://doi.org/10.1016/j.earscirev.2025.105237

Muñoz J.A., 1992. Evolution of a continental collision belt: ECORS-Pyrenees crustal balanced cross-section. In: McClay K.R. (Ed.), *Thrust Tectonics*, 235–246. Chapman and Hall, London, U.K.

Muñoz J.A., 2002. The Pyrenees. In: Gibbons W. and Moreno T. (Eds), *The Geology of Spain*, 370–385. Geological Society, London, U.K.

Norris D.K. and Black R.F., 1961. Application of palaeomagnetism to thrust mechanics. *Nature*, **192**, 933–935, https://doi.org/10.1038/192933a0

Nye J.F., 1957. *Physical Properties of Crystals*. Oxford University Press, Oxford, U.K.

Oliva-Urcia B. and Pueyo E.L., 2007. Rotational basement kinematics deduced from remagnetized cover rocks (Internal Sierras, southwestern Pyrenees). *Tectonics*, **26**, TC4014, https://doi.org/10.1029/2006TC001955

Oliva-Urcia B., Casas A.M., Pueyo E.L. and Pocoví A., 2012. Structural and paleomagnetic evidence for non-rotational kinematics in the western termination of the External Sierras (southwestern central Pyrenees). *Geol. Acta*, **10**, 125–144, https://doi.org/10.1344/105.000001704

Oliva-Urcia B., Beamud E., Arenas C., Pueyo E.L., Garcés M., Soto R., Valero L. and Pérez-Rivarés F.J., 2019. Dating the northern deposits of the Ebro foreland basin, kinematics of the frontal deformation in the SW Pyrenees. *Tectonophysics*, **765**, 11–34, https://doi.org/10.1016/j.tecto.2019.05.007

Parés J.M., van der Pluijm B. and Dinarès-Turell J., 1999. Evolution of magnetic fabrics during incipient deformation of mudrocks (Pyrenees, northern Spain). *Tectonophysics*, **307**, 1–14, https://doi.org/10.1016/S0040-1951(99)00115-8

Parés J.M., 2004. How deformed are weakly deformed mudrocks? Insights from magnetic anisotropy. Martín-Hernández F., Lüneburg C.M., Aubourg C. and Jackson M. (Eds), *Magnetic Fabric, Methods and Applications*. *Geol. Soc. London Spec. Publ.*, **238**, 191–203, https://doi.org/10.1144/GSL.SP.2004.238.01.13

Parés J.M., 2015. Sixty years of anisotropy of magnetic susceptibility in deformed sedimentary rocks. *Front. Earth Sci.*, **3**, Art.No.4, https://doi.org/10.3389/feart.2015.00004

Pedrera A., García-Senz J., Pueyo E.L., López-Mir B., Silva-Casal R. and Díaz-Alvarado J., 2023. Inhomogeneous rift inversión and the evolution of the Pyrenees. *Earth Sci. Rev.*, **245**, Art.No.104555, https://doi.org/10.1016/j.earscirev.2023.104555

Pocoví A., Pueyo Anchuela Ó., Pueyo E.L., Casas-Sainz A.M., Román Berdiel M.T., Gil Imaz A., Ramajo Cordero J., Mochales T., García Lasanta C., Izquierdo E., Parés J.M., Sánchez E., Soto Marín R., Oliván C., Rodríguez Pintó A., Oliva-Urcia B. and Villalaín J.J., 2014. Magnetic fabrics in the Central-Western Pyrenees: An overview. *Tectonophysics*, **629**, 303–318, https://doi.org/10.1016/j.tecto.2014.03.027

Pueyo E.L., Millán H. and Pocoví A., 2002. Rotation velocity of a thrust: a paleomagnetic study in the External Sierras (Southern Pyrenees). *Sediment. Geol.*, **146**, 191–208, https://doi.org/10.1016/S0037-0738(01)00172-5

Pueyo E.L., Oliva-Urcia B., Sussman A.J. and Cifelli F., 2016. Palaeomagnetism in fold and thrust belts: Use with caution. In: Pueyo E.L., Cifelli F., Sussman A. and Oliva-Urcia B. (Eds), *Palaeomagnetism in Fold and Thrust Belts: New Perspectives*. *Geol. Soc. London Spec. Publ.*, **425**, 259–276, https://doi.org/10.1144/SP425.14

Pueyo E.L., Oliva-Urcia B., Sánchez-Moreno E.M., Arenas C., Silva-Casal R., Calvín P., Santolaria P., García-Lasanta C., Oliván C., Compaired F., Casas A.M. and Pocoví A., 2021. The geometry and kinematics of the Southwestern termination of the Pyrenees; A field guide to the Sto. Domingo anticline. In: Mukherjee S. (Ed.), *Structural Geology and Tectonics Field Guidebook*, Vol. 1, 49–101. Springer, Cham, Switzerland, https://doi.org/10.1007/978-3-030-60143-0_3

Pueyo E.L., Rodríguez-Pintó A., Serra-Kiel J. and Barnolas A., 2022. The chronology and rotational kinematics in the South-Eastern Jaca Basin (Southern Pyrenees): Las Bellostas section. *Geol. Acta*, **20**, 1–29, https://doi.org/10.1344/GeologicaActa2022.20.12

Pueyo E.L., Calvín P., Egli R., Izquierdo-Llavall E., Beamud E., Sierra-Campos P., Oliva-Urcia B., Rodríguez-Pintó A., Mata M.P. and Larrasoaña J.C. 2024. Cinemática de la rotación y remagnetización en la Cuenca de Jaca. *Geotemas*, **20**, 197–197 (in Spanish)

Pueyo E.L., Santolaria P., Calvín P., Casas A.M., Sánchez E., Oliva-Urcia B., Silva-Casal R., Scholger R, Rubio F., Rey-Moral C., Rodríguez-Pintó A., Ayala C., Egli R. and Pocoví A., 2025. Vertical-axis rotations and salt tectonics in the southwestern Pyrenean termination. In: Iriondo A., Lawton T., Geissman J. (Eds), *Special Paper Devoted to Roberto Molina-Garza*. Geological Society of America, in print

Pueyo-Anchuela Ó., Casas-Sainz A.M., Pocoví-Juan A. and Gil-Imaz A., 2011. Lithology-dependent reliability of AMS analysis: A case study of the Eocene turbidities in the southern Pyrenees (Aragón, Spain). *C. R. Geosci.*, **343**, 11–19, https://doi.org/10.1016/j.crte.2010.11.003

Pueyo-Anchuela Ó., Pueyo E.L., Casas-Sainz A.M., Pocoví-Juan A. and Gil-Imaz A., 2012. Vertical axis rotations in fold and thrust belts: comparison of AMS and paleomagnetic data in the Western External Sierras (Southern Pyrenees). *Tectonophysics*, **532**, 119–133, https://doi.org/10.1016/j.tecto.2012.01.023

Pueyo-Anchuela Ó., Casas A.M., Pueyo E.L., Pocoví A. and Gil-Imaz A., 2013. Analysis of the ferromagnetic contribution to the susceptibility by low field and high field methods in sedimentary rocks of the Southern Pyrenees and Northern Ebro foreland basin (Spain). *Terra Nova*, **25**, 307–314, https://doi.org/10.1111/ter.12037

Puigdefábregas C.T., 1975. *La sedimentacion molasica en la cuenca de Jaca*. Pirineos, 104, 188 pp. (in Spanish)

Ramón M.J., Pueyo E.L., Oliva-Urcia B. and Larrasoaña J.C., 2017. Virtual directions in paleomagnetism: a global and rapid approach to evaluate the NRM components. *Front. Earth Sci.*, **5**, Art. No.8, https://doi.org/10.3389/feart.2017.00008.

Robador Moreno A., Ramajo Cordero J., Muñoz Jiménez A., Pérez García A., Luzón Aguado A., Arenas Abad C. and González Rodríguez A., 2024a. *Mapa Geológico Digital continuo E. 1: 50.000, Zona Cuenca del Ebro (Zona-2700)*, http://info.igme.es/cartografiadigital/geologica/geodezona.aspx?Id=Z2700

Robador Moreno A., Samsó Escola J.M., Ramajo Cordero J., Barnolas Cortinas A., Clariana García P., Martín Alfageme S. and Gil Peña I. 2024b. *Mapa Geológico Digital continuo E. 1:50.000, Zona Pirineos Vasco-Cantábrica (Zona-1600)*, http://info.igme.es/cartografiadigital/geologica/geodezona.aspx?Id=Z1600

Rodríguez-Pintó A., Pueyo E.L., Calvín P., Sánchez E., Ramajo J., Casas A.M. and Román T., 2016. Rotational kinematics of a curved fold: The Balzes anticline (Southern Pyrenees). *Tectonophysics*, **677**, 171–189, https://doi.org/10.1016/j.tecto.2016.02.049

Sagnotti L., Speranza F., Winkler A., Mattei M. and Funiciello R., 1998. Magnetic fabric of clay sediments from the external northern Apennines (Italy). *Phys. Earth Planet. Inter.*, **105**, 73–93, https://doi.org/10.1016/S0031-9201(97)00071-X

Sierra-Campos P., Calvín P., Izquierdo-Llavall E., Pérez-Landazábal J.I., Montes M., Luzón A., Bellido E., Pueyo E.L. and Larrasoaña J.C. 2025a. Magnetic fabrics of weakly-deformed mudrocks from the Jaca-Pamplona basin (Pyrenees); new constrains on the sensitivity of magnetic fabrics and the tectonic evolution of the Southern Pyrenees. *J. Iber. Geol.*, **51**, 283–301, https://doi.org/10.1007/s41513-025-00288-8

Sierra-Campos P., Pueyo E.L., Calvín P., Montes M., Luzón A., Bernaola G., Mata M.P., Bellido E., Beamud E., Scholger R. and Larrasoaña J.C., 2025b. Bartonian-Priabonian rotational evolution of the central Jaca-Pamplona Basin, Southern Pyrenees. *Geogaceta*, **77**, 27–30, https://doi.org/10.55407/geogaceta108766

Soto R., Larrasoaña J.C., Arlegui L.E., Beamud E., Oliva-Urcia B. and Simón J.L., 2009. Reliability of magnetic fabric of weakly deformed mudrocks as a palaeostress indicator in compressive settings. *J. Struct. Geol.*, **31**, 512–522. https://doi.org/10.1016/j.jsg.2009.03.006

Tarling D.H. and Hrouda F., 1993. *The Magnetic Anisotropy of Rocks*. Chapman and Hall, London, U.K.

Teixell A., Labaume P. and Lagabrielle Y., 2016. The crustal evolution of the west-central Pyrenees revisited: Inferences from a new kinematic scenario. *C. R. Geosci*, **348**, 257–267, https://doi.org/10.1016/j.crte.2015.10.010

Teixell A., 1996. The Ansó transect of the southern Pyrenees: Basement and cover thrust geometries. *J. Geol. Soc.*, **153**, 301–310, https://doi.org/10.1144/gsjgs.153.2.0301

Teixell A., 1998. Crustal structure and orogenic material budget in the west central Pyrenees. *Tectonics*, **17**, 395–406, https://doi.org/10.1029/98TC00561

Toro M.R., Sáinz A.M.C., Llavall E.I., Morer E.L.P., Navas J., Medina C.P. and Martín J. 2021. Geometría del basamento Pirenaico Suroccidental a partir de la exploración sísmica. *Geotemas*, **18**, 565–565 (in Spanish)

Toro M.R., 2025. *Modelización 2D y 3D de la zona Surpirenaica Occidental: implicaciones estructurales y en los recursos del subsuelo*. Ph.D. Thesis. Universidad de Zaragoza, Zaragoza, Spain (in Spanish)

Weaver R., Roberts A.P., Flecker R. and MacDonald D.I.M., 2004. Tertiary geodynamic of Sakhalin (NW Pacific) from anisotropy of magnetic susceptibility fabrics and paleomagnetic data. *Tectonophysics*, **379**, 25–42, https://doi.org/10.1016/j.tecto.2003.09.028

Zijderveld J.D.A., 1967. A.C. demagnetization of rocks: Analysis of results. In: Runcorn S.K., Creer K.M. and Collinson D.W. (Eds), *Methods in Palaeomagnetism*, 254–286. Elsevier, Amsterdam, The Netherlands, https://doi.org/10.1016/B978-1-4832-2894-5.50049-5

Authors and Affiliations

Pablo Sierra-Campos[1,2] · Pablo Calvín[3] · Esther Izquierdo-Llavall[1,2] · Manuel Montes[4] · Aránzazu Luzón[2,5] · Eva Bellido[4] · Elisabet Beamud[6] · Emilio L. Pueyo[1,2] · Juan Cruz Larrasoaña[1,2,7]

✉ Juan Cruz Larrasoaña
jc.larra@igme.es

Pablo Sierra-Campos
p.sierra@igme.es

Pablo Calvín
pcalvin@usal.es

Esther Izquierdo-Llavall
e.izquierdo@igme.es

Manuel Montes
m.montes@igme.es

Aránzazu Luzón
aluzon@unizar.es

Eva Bellido
e.bellido@igme.es

Elisabet Beamud
betbeamud@ub.edu

Emilio L. Pueyo
unaim@igme.es

1 CN IGME, CSIC, Unidad de Zaragoza, Avenida Montañana 1005, 50059 Zaragoza, Spain

2 Unidad Asociada en Ciencias de La Tierra, Universidad de Zaragoza, C/Pedro Cerbuna 12, 50009 Zaragoza, Spain

3 Departamento de Geología, Universidad de Salamanca, Salamanca, Spain

4 CN IGME, CSIC, Ríos Rosas 23, 28003 Madrid, Spain

5 Departamento de Ciencias de La Tierra, Geotransfer-IUCA, Universidad de Zaragoza, C/Pedro Cerbuna 12, 50009 Zaragoza, Spain

6 Paleomagnetic Laboratory CCiTUB-GEO3BCN CSIC, C/Lluis Solé I Sabarís S/N, 08028 Barcelona, Spain

7 Departamento de Ciencias, Universidad Pública de Navarra, Pamplona, Spain